

The anisotropic and rheological structure of the oceanic upper mantle from a simple model of plate shear

Noah S. Podolefsky, Shijie Zhong and Allen K. McNamara

Department of Physics, University of Colorado at Boulder, Boulder, CO 90309, USA. E-mail: szhong@anquetil.colorado.edu (SZ)

Accepted 2004 January 15. Received 2004 January 7; in original form 2003 July 28

SUMMARY

We have developed a channel flow model that dynamically couples plate motion and mantle stress with a composite rheology (diffusion creep and dislocation creep) to study the rheological and anisotropic structures of the oceanic upper mantle. A semi-analytic approach is used to solve for mantle stress and viscosity, allowing fast calculations and exploration of a wide range of rheological parameters. Mantle stress in our model is due to shearing by a moving plate. By comparing mantle stress with a transition stress for dislocation creep, we identify regions where either diffusion creep or dislocation creep is active. Deformation by dislocation creep results in a mineral fabric that may be responsible for observed seismic anisotropy. Our study suggests that there is an important relation between plate motion, seismic anisotropy, mantle viscosity and transition stress. Using laboratory results for rheological parameters, we find that dislocation creep exists only in a layer at certain depths in the upper mantle. For a plate velocity of 10 cm yr^{-1} , an asthenospheric viscosity of 10^{19} Pa s and an asthenospheric transition stress of 0.1 MPa , our model predicts a $\sim 200 \text{ km}$ thick dislocation creep layer, which is broadly consistent with the observations of seismic anisotropy. For a plate velocity of 10 cm yr^{-1} and an asthenospheric transition stress of 0.1 MPa , the asthenospheric viscosity needs to be greater than $5 \times 10^{18} \text{ Pa s}$ to produce any dislocation creep deformation, and the asthenospheric viscosity needs to be larger for slower plate motion or larger transition stress. Slower plate motion leads to a thinner dislocation creep layer, which may partially explain the observed asymmetry in anisotropic structure in the East Pacific Rise.

Key words: anisotropy, dislocation creep, plate shear, rheology.

1 INTRODUCTION

Our understanding of oceanic upper mantle seismic anisotropy has improved greatly over recent years with the use of different seismic techniques. For example, surface wave studies have shown that the central Pacific is characterized by unusually large radial anisotropy (Ekstrom & Dziewonski 1998) with fast directions of azimuthal anisotropy largely parallel to plate motion (Montagner 2002). However, observations of anisotropy are more complicated in the older regions of the Pacific Plate, exhibiting lower magnitudes in addition to directions not parallel to plate motion (Montagner 2002; Becker *et al.* 2003). Using *SKS* and *SKKS* shear wave splitting, Wolfe & Solomon (1998) observed ridge-perpendicular anisotropy on both sides of the East Pacific Rise (EPR). They found that the magnitude of anisotropy on the faster-moving Pacific Plate is twice that of the slower Nazca Plate, hinting at a relationship between plate velocity and degree of anisotropy.

Theoretical (Wenk & Christie 1991; Ribe 1992; Blackman *et al.* 2002) and laboratory (Nicolas & Christensen 1987; Karato & Wu 1993; Zhang & Karato 1995) studies have shown that the formation of seismic anisotropy is intimately linked to both mantle rhe-

ology and the mantle flow field. These studies have found that the two primary mechanisms of upper mantle deformation are diffusion creep and dislocation creep. While both are thought to occur simultaneously, the dominating mechanism is controlled by the magnitude of tectonic stress. Diffusion creep is characterized by diffusion of atoms along grain boundaries and dominates under lower stresses, whereas dislocation occurs by the slipping along crystallographic glide planes and dominates at higher stresses. Diffusion creep produces randomly aligned crystallographic directions, resulting in a seismically isotropic aggregate. Dislocation creep, on the other hand, tends to align individual crystals, resulting in a seismically anisotropic aggregate in which the direction and magnitude of anisotropy is related to the flow direction and amount of strain accommodated by dislocation creep respectively. The resulting fabric of the mineral grains is referred to as the lattice-preferred orientation (LPO) and is thought to be responsible for the observed seismic anisotropy of the upper mantle (e.g. Dziewonski & Anderson 1981; Montagner & Tanimoto 1991).

Therefore, seismic anisotropy and the deformation mechanism are inherently related (Karato & Wu 1993), with two controlling parameters: tectonic stress and transition stress. Transition stress

is defined as the stress at which dislocation and diffusion creep mechanisms accommodate an equal amount of strain. Diffusion (dislocation) creep is the primary deformation mechanism when tectonic stress is below (above) the transition stress (e.g. Karato & Wu 1993; Hirth & Kohlstedt 2003). While transition stress is determined by rheological parameters and pressure and temperature conditions (Karato & Wu 1993), tectonic stress is controlled by mantle deformation and viscosity. Since mantle viscosity depends on tectonic stress for dislocation creep because of its stress dependence, tectonic stress may also depend on the primary deformation mechanism or transition stress.

For oceanic upper mantle in particular, where the strain rate may be estimated to first order from plate motion, the tectonic stress is sensitive to asthenospheric viscosity. Asthenospheric viscosity has important implications for mantle and crustal dynamics, including the onset time of small-scale convection (Davaille & Jaupart 1994), long-wavelength geoid and heat flux (Hager 1991) and post-seismic deformation (e.g. Pollitz *et al.* 1998). Asthenospheric viscosity can be estimated using different observations and models but with significant uncertainties, ranging from 5×10^{17} Pa s (Pollitz *et al.* 1998) to 2×10^{19} Pa s (Hager 1991) or larger (Korenaga & Jordan 2002; Zhong & Watts 2002). Clearly, too small an asthenospheric viscosity may not produce a large enough mantle stress to create dislocation creep deformation and seismic anisotropy in the oceanic upper mantle. Therefore, we think that a careful understanding of rock deformation processes is important if we are to use observations of seismic anisotropy in the upper mantle to constrain asthenospheric viscosity and to infer mantle flow structure.

Several studies have taken advantage of this relationship between seismic anisotropy and flow direction to shed new light onto the dynamics of upper mantle flow. McKenzie (1979) was the first to study this relationship in terms of convective flow at ridges and subduction zones. Kubo & Hiramatsu (1998) examined seismic anisotropy below continents. They suggested that shear deformation in the asthenosphere due to present plate motion could produce anisotropy in addition to frozen-in anisotropy in the lithosphere. Wolfe & Solomon (1998) suggested that the asymmetry in the delay times may be caused by the asthenospheric return flow. Assuming that fast shear wave polarization of mantle minerals aligns with the orientation of maximum extensional strain, and using global mantle flow models to simulate the strain pattern, Becker *et al.* (2003) and Gaboret *et al.* (2003) proposed that the Pacific anisotropy structure can be explained in terms of mantle deformation caused by plate motion and mantle buoyancy. With similar assumptions, shear wave splitting data are used to infer the mantle flow below the western United States and Iceland (Silver & Holt 2002; Bjarnason *et al.* 2002). These studies have typically relied upon modelling the flow fields based on Newtonian rheology, inconsistent with dislocation creep. However, since the flow fields produced by both Newtonian and non-Newtonian rheologies are likely to be similar, if the main goal is to derive directional information about the flow field, this approach may represent a reasonable approximation. Using a more realistic composite rheology that takes both diffusion and dislocation creep into account (e.g. Parmentier *et al.* 1976; Van den Berg *et al.* 1993; Hall & Parmentier 2003) may determine mantle stress and transition stress dynamically. Regions of dislocation creep deformation or seismic anisotropy can then be determined. For example, McNamara *et al.* (2002, 2003) used a composite rheology to constrain the formation of LPO to certain regions in the lowermost mantle.

Here we investigate the controls on deformation mechanisms and viscosity structure in the oceanic upper mantle and their implica-

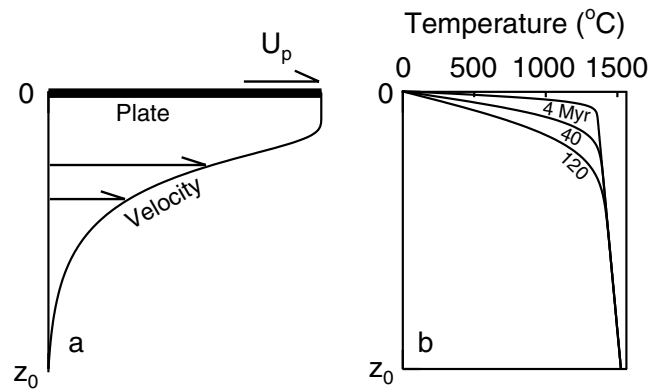


Figure 1. (a) Channel flow model with a rigid plate moving with uniform velocity, U_p , over a viscous mantle. (b) Temperature curves for three lithospheric ages.

tions for seismic anisotropy by using a composite rheology in a simple Couette flow driven by surface plate motion. The motivation for this work is two-fold. First, we examine how the seismic anisotropy of the oceanic upper mantle along with mineral physics constraints on transition stress can be used to place lower bounds on asthenospheric viscosity. For example, to develop LPO, mantle stresses must be greater than the transition stress, which is difficult to achieve if mantle viscosity is too low. Secondly, we examine how the strength of predicted anisotropy varies with lithospheric age and how it compares with the observations of Pacific anisotropy. Specifically, we investigate whether our simple plate shearing model can explain the reduction of anisotropy magnitude in the older portions of the Pacific, as observed in Montagner (2002).

Our study represents an extension of that of Karato & Wu (1993) in which we vary rheological parameters (e.g. activation energies and volumes for dislocation creep and diffusion creep) to determine how transition stress may vary with the depth and age of the oceanic lithosphere. However, different from Karato & Wu (1993), mantle stress in our study, that determines zones of dislocation creep by comparison with transition stress, is dynamically coupled with plate motion and viscosity structure through non-linear composite rheology. We focus our attention on identifying the depth ranges and strength of dislocation creep deformation in the upper mantle that is induced by plate shear. We also examine the spatial and temporal distribution of strain accommodated by dislocation creep to investigate whether LPO is either destroyed or ‘frozen-in’ as plate age increases. Furthermore, we use the more up to date experimental data in Karato & Jung (2003) and Hirth & Kohlstedt (2003). While our approach does not allow for the determination of a 3-D strain field as in Becker *et al.* (2003) and Gaboret *et al.* (2003), our semi-analytic formulation has the advantage over fully dynamic calculations (e.g. McNamara *et al.* 2002, 2003) in that it allows us to explore the non-linear dynamics over an extensive parameter space for plate motion, mantle viscosity and activation parameters.

2 MODEL

We consider a 1-D channel flow model commonly known as Couette flow in which the surface moves with uniform velocity over a viscous medium (Fig. 1a). Boundary conditions are constant plate velocity, U_p , at the top and zero velocity at $z = z_0$. We assume that horizontal pressure gradients can be ignored, which, to first order, is justified for the asthenosphere below large plates such as the Pacific Plate.

With this assumption, the shear stress is constant with depth and is dependent on viscosity and the vertical gradient of the horizontal velocity (e.g. Turcotte & Schubert 2002). By coupling this tectonic stress with a composite rheology that determines transition stress for dislocation creep, τ_T , we can determine the interdependence of plate motion, zones of dislocation creep, asthenospheric viscosity and other rheological parameters.

For Couette flow with viscosity that depends only on the vertical coordinate, z , the momentum equation can be expressed as,

$$\tau = \eta \frac{\partial u}{\partial z} = \text{constant}, \quad (1)$$

where τ is the shear stress, η is viscosity and u is horizontal velocity. We can write the stress as,

$$\tau = U_p \left(\int_{z_0}^0 \frac{1}{\eta} dz \right)^{-1}. \quad (2)$$

A general expression for mantle rheology (e.g. Karato & Wu 1993; Karato & Jung 2003; Hirth & Kohlstedt 2003) is,

$$\dot{\epsilon}_i = A_i d^{-m_i} C_{\text{OH}}^{r_i} \tau^n \exp\left(-\frac{E_i + P V_i}{RT}\right), \quad (3)$$

where $\dot{\epsilon}_i$ is strain rate, the subscript i denoting the deformation mechanism with f and l representing diffusion and dislocation creep respectively, A_i is a prefactor, d is the grain size, m is the grain size exponent, C_{OH} is the water content, r is the water content exponent, E_i is the activation energy, P is the pressure, V_i is the activation volume, R is the universal gas constant, T is temperature and n is the stress exponent. For a system closed to water, C_{OH} is constant and eq. (3) is valid for wet conditions (Karato & Jung 2003). For diffusion creep, $n = 1$, while for dislocation creep $n \sim 3.5$ (e.g. Karato & Wu 1993). Since grain size evolution and water concentration in the mantle are not well constrained, we absorb the effects of grain size and water concentration into the prefactor, which is treated as a variable. In this study, temperature in the oceanic upper mantle is given by a half-space cooling model with an adiabatic temperature gradient of 0.3 K km^{-1} superimposed (e.g. Turcotte & Schubert 2002) (Fig. 1b).

The viscosity is determined by a composite rheology in which contributions from diffusion and dislocation creep mechanisms are assumed to be cumulative (Parmentier *et al.* 1976; Van den Berg *et al.* 1993; McNamara *et al.* 2002; Hirth & Kohlstedt 2003). The total strain rate can be written as,

$$\dot{\epsilon} = \dot{\epsilon}_f + \dot{\epsilon}_l, \quad (4)$$

and the effective viscosity can be expressed as,

$$\eta = \left[A_f \exp\left(-\frac{E_f + P V_f}{RT}\right) + A_l \tau^{n-1} \exp\left(-\frac{E_l + P V_l}{RT}\right) \right]^{-1}. \quad (5)$$

The transition stress can be defined as the stress at which $\dot{\epsilon}_f = \dot{\epsilon}_l$,

$$\tau_T = \left[\frac{A_f}{A_l} \exp\left(\frac{(E_l - E_f) + P(V_l - V_f)}{RT}\right) \right]^{\frac{1}{n-1}}. \quad (6)$$

The viscosity can be rewritten in terms of τ_T as,

$$\eta = \frac{1}{A_f} \exp\left(\frac{E_f + P V_f}{RT}\right) \left[1 + \left(\frac{\tau}{\tau_T}\right)^{n-1} \right]^{-1}. \quad (7)$$

Although E_l and V_l do not appear explicitly in (7) for η , the dependence of η on them is retained in τ_T . The prefactors A_l and A_f

Table 1. Physical parameters.

Mantle density	3300 kg m ⁻³
Universal gas constant	8.3 J mol ⁻¹ K ⁻¹
Dislocation creep activation energy	480 × 10 ³ J mol ⁻¹
Diffusion creep activation energy	335 × 10 ³ J mol ⁻¹
Diffusion creep activation volume	4 cm ³ mol ⁻¹
Gravitational acceleration	9.8 m s ⁻²
Model depth (z_0)	600 km
Stress exponent	3.5

are chosen so that τ_T and η have the reference values τ_{Tref} and η_{Tref} at $z = z_0$. Both τ_T and η vary with depth due to their dependence on pressure and temperature. However, η also depends on tectonic stress τ (see eq. 7), which is dependent on plate motion in our model (eq. 2). z_0 is taken as 600 km in this study. However, our tests with $z_0 = 800$ km show that our results are insensitive to this parameter, because as we will show later, strain rate is largely concentrated in the asthenosphere where the viscosity is small.

Eqs (2) and (7) together form a non-linear relationship between stress and viscosity. For a given mantle temperature profile (or lithospheric age t_{li}), plate motion U_p , rheological parameters including activation parameters, τ_{Tref} and η_{Tref} , a solution for stress and viscosity is found by an iterative procedure. An initial viscosity profile is calculated from eq. (7) by assuming $\tau = 0$. From the updated η and eq. (2), a new value is found for τ , which is then used in eq. (7) to calculate a new viscosity profile. Repeating this procedure converges upon the solution. Given the solution of stress and viscosity, we can identify zones of dislocation creep (i.e. where $\tau > \tau_T$) and diffusion creep (i.e. where $\tau < \tau_T$) and examine how the regions of dislocation creep depend on rheological parameters including asthenospheric viscosity.

We wish to point out how our approach differs from that of Karato & Wu (1993). In their study, Karato & Wu (1993) considered eq. (3) with the prefactors, A_i , as constants, but grain size, d , and stress were treated as variables. In our approach, plate motion and viscosity control stress via eq. (2), while grain size is implicit in the prefactors. While treating d and τ as variables is reasonable in the context of laboratory studies, for our purposes considering parameters more directly related to mantle dynamic models (i.e. η_{Tref} and τ_{Tref}) as variables is more appropriate. We assume that d is constant for a fixed set of rheological parameters, but it can change as the parameters are varied. To estimate the grain size, η_{Tref} can be related directly to d by comparing eq. (3) with eq. (7). We obtain,

$$d = \left[A_f \eta_{\text{Tref}} C_{\text{OH}}^{r_f} \exp\left(-\frac{E_f + \rho g z_0 V_f}{RT_0}\right) \right]^{1/m}. \quad (8)$$

where T_0 is the temperature at $z = z_0$, ρ is the mantle density and g is gravitational acceleration. As an example, Hirth & Kohlstedt (2003) provide the values $A_f = 1 \mu \text{ m}^3 \text{ Pa s}^{-1}$, $C_{\text{OH}} = 1000 \text{ H}/10^6 \text{ Si}$, $m = 3$ and $r = 1.0$ for diffusion creep. Using these values along with those from Table 1 and $\eta_{\text{Tref}} = 10^{21} \text{ Pa s}$, we obtain $d = 10 \text{ mm}$. This value of grain size is similar to values suggested in other studies (Karato & Wu 1993; Hirth 2002; Hirth & Kohlstedt 2003). We should point out that if the prefactors for both diffusion and dislocation creep are held constant, as in Karato & Wu (1993), η_{Tref} and τ_{Tref} should both depend on grain size and on each other. However, we relax this constraint and treat η_{Tref} and τ_{Tref} as independent parameters.

3 RESULTS

The zones of dislocation creep in the oceanic upper mantle are controlled by transition stress τ_T which has depth dependence

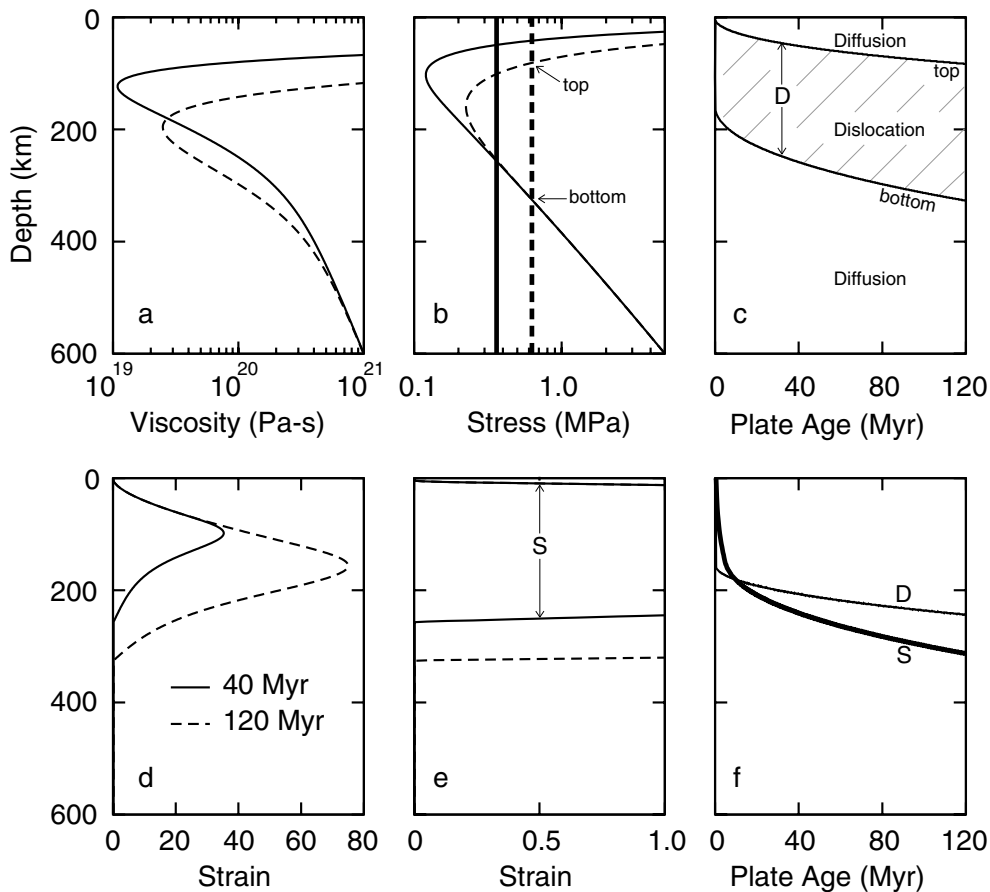


Figure 2. A reference case with $\eta_{\text{ref}} = 10^{21}$ Pa s, $\tau_{\text{Tref}} = 5$ MPa, $V_1 = 14$ cm³ mol⁻¹, and $U_p = 10$ cm yr⁻¹. Solid and dashed lines are for ages 40 Myr and 120 Myr respectively. (a) Temperature-, pressure- and stress-dependent viscosity. (b) Shear stress (thick vertical lines); transition stress (thin curved lines). (c) Top and bottom of layer D versus plate age. The hatched area is the dislocation creep channel D. (d) Accumulated strain in the dislocation creep channel. (e) Blow-up of strain curves in (d) from 0–1.0. (f) Layer thickness for layers D and S versus plate age. The vertical axis is layer thickness rather than depth.

determined by rheological parameters, and tectonic stress, which in the current study is determined by plate motion U_p in addition to rheological parameters. We use experimentally determined activation energies E_1 and E_f from Hirth & Kohlstedt (2003), which seem rather robust from different laboratory studies (see Table 1). Following Karato & Wu (1993), we fix activation volume for diffusion creep V_f , while treating V_1 as a variable. Other fixed parameters in our study are given in Table 1. We use activation parameters appropriate for the wet conditions, but we also consider cases in which the viscosity in the top 70 km is increased as a result of dehydration and melting at spreading centres where the oceanic crust is generated (Karato 1986; Hirth & Kohlstedt 1996). We explore the effects of varying η_{ref} , τ_{Tref} , V_1 , U_p , and t_{li} (lithospheric age) on the dynamics and the zone of dislocation creep.

3.1 A reference case

We first present a reference case in which $U_p = 10$ cm yr⁻¹, $V_1 = 14$ cm³ mol⁻¹, $\tau_{\text{Tref}} = 5$ MPa and $\eta_{\text{ref}} = 10^{21}$ Pa s. $\eta_{\text{ref}} = 10^{21}$ Pa s (i.e. the viscosity at 600 km depth) is chosen here to mimic the viscosity increase from the upper mantle to the lower mantle that is inferred from the post-glacial rebound and long-wavelength geoid studies (Hager & Richards 1989; Simons & Hager 1997; Forte & Mitrovica 1997). We recognize that the transition zone viscosity is not well constrained (e.g. Simons & Hager 1997), and different η_{ref} will be considered later. τ_{Tref} is chosen here because it produces τ_T

in the range of 0.1–1 MPa in asthenosphere as suggested by Hirth & Kohlstedt (2003).

For $t_{\text{li}} = 40$ Myr, the solutions of viscosity and stress are given in Figs 2(a) and (b) (solid lines). While the viscosity is depth-dependent with a minimum viscosity of $\sim 10^{19}$ Pa s at ~ 125 km depth in the asthenosphere, the stress is constant at all depths and is ~ 0.35 MPa (solid vertical line in Fig. 2b). At shallow depths, viscosity is dominated by the activation energy (E_f) term (see eq. 7) and increasing temperature causes viscosity to decrease with depth (Fig. 2a). At large depths, where the temperature increase is small, the pressure term controls the viscosity. Hence, viscosity has a minimum in the asthenosphere and increases with depth in the deep upper mantle.

Since we use different values of the activation energy and volume for diffusion and dislocation creep, transition stress, τ_T , is temperature- and pressure-dependent and shows a similar depth dependence to viscosity. For $t_{\text{li}} = 40$ Myr, τ_T is ~ 0.12 MPa in the asthenosphere and increases to $\tau_T = 5$ MPa at $z = z_0$ (curved line in Fig. 2b). At depths shallower than 50 km or larger than 260 km, mantle stress is less than τ_T and diffusion creep deformation dominates (Fig. 2b). At depths between 50 km and 260 km, stress is larger than τ_T and dislocation creep dominates in a channel ~ 210 km thick.

As lithosphere ages, the upper mantle cools, causing mantle viscosity to increase at shallow depths. For this reference case with $t_{\text{li}} = 120$ Myr, the minimum viscosity becomes $\sim 2.5 \times 10^{19}$ Pa s and it occurs at a depth of 200 km (dashed line in Fig. 2a). Since

temperature in the deep upper mantle changes little with time, viscosity in the deep upper mantle remains unchanged. For the given plate motion, the overall increase in viscosity for $t_{li} = 120$ Myr leads to larger mantle stress, compared with that for $t_{li} = 40$ Myr (vertical lines in Fig. 2b). The increased stress causes a reduction in viscosity at the intermediate depths because of the non-linear viscosity (see eq. 7). The decreased temperature has similar effects on τ_T as on viscosity (Fig. 2b). τ_T for $t_{li} = 120$ Myr is larger at shallow depths but remains unchanged at larger depths, compared with those for $t_{li} = 40$ Myr (Fig. 2b). For $t_{li} = 120$ Myr, dislocation creep occurs between 80 km and 330 km depths. For this reference case, as t_{li} increases, both the thickness and depth of dislocation creep channel increase (Fig. 2c where D is the thickness of the channel where dislocation creep dominates).

Strain in the dislocation creep channel creates an LPO that is responsible for seismic anisotropy (e.g. Karato & Wu 1993). To better relate our model to the strength of seismic anisotropy, we calculated accumulated strain from dislocation creep in the mantle for different lithospheric ages t_{li} (Figs 2d–e). Ignoring 2-D effects, for a given z we integrated strain rate with time to t_{li} for depths where mantle stress has been greater than τ_T (i.e. in the dislocation creep channel). For $t_{li} = 40$ Myr, the accumulated strain remains negligibly small at depths smaller than 5 km but increases rapidly at depths greater than 5 km. The accumulated strain is as large as 30 at a depth of ~ 100 km and decreases rapidly at a depth of ~ 260 km where diffusion creep becomes dominant (Fig. 2d). Although for $t_{li} = 40$ Myr the dislocation creep channel starts at a depth of 50 km (Fig. 2b), the accumulated strain due to dislocation creep deformation is significant at 5 km depth (Fig. 2e). This is because the dislocation creep channel starts at shallower depths for smaller lithospheric age (Fig. 2c). Diffusion creep tends to destroy the LPO, but we find that at shallow depths, the deformation mechanism switches from dislocation creep to diffusion creep for increasing age, and the viscosity becomes sufficiently large such that diffusion creep produces insignificant strain. It is therefore possible that LPO can become ‘frozen-in’ and remain in a region where diffusion creep currently dominates but where material was previously subjected to dislocation creep deformation. For $t_{li} = 120$ Myr, the accumulated strain increases and the layer with significant accumulated strain also increases.

We define layer S in which the accumulated strain due to dislocation creep is greater than 0.5 (Fig. 2e). Modelling deformation of grain aggregates suggests that after the strain is greater 0.5, the strength of the anisotropy does not increase with further strain (Ribe 1992). Therefore the thickness of layer S in our model provides a measure for the strength of anisotropy in the upper mantle. At young ages, layer S is thinner than layer D since sufficient strain to produce LPO has not accumulated (Fig. 2f). However, the thickness of layer S increases with age. After 20 Myr, it is larger than the thickness of dislocation creep channel D , because of the freezing-in effect mentioned above.

3.2 Effects of varying U_p , V_1 , τ_{Tref} , and η_{ref}

We first examine the effects of varying plate motion U_p . Figs 3(a), (b) and (c) show a comparison of the reference case to calculations in which U_p is reduced from 10 cm yr⁻¹ to 5 cm yr⁻¹ but other parameters are the same as in the reference case. Close inspection of results for $t_{li} = 40$ Myr reveals that shear stress does not scale linearly with plate velocity (Fig. 3b). From eq. (2), shear stress decreases with decreasing U_p . However, due to its stress dependence

(eq. 7), the viscosity increases with decreasing stress (Fig. 3a), causing a non-linear change of stress with U_p . The thickness of layer S is reduced overall, but the percentage change in S due to change in U_p is larger for young lithosphere than for old lithosphere (Fig. 3c).

Figs 3(d), (e) and (f) show results of varying η_{ref} while other parameters are kept the same as in the reference case. For $\eta_{ref} = 10^{20}$ Pa s and $t_{li} = 40$ Myr, shear stress is reduced (Fig. 3e) and the thickness of layer S is also reduced (Fig. 3f). Increasing η_{ref} increases shear stress. For $\eta_{ref} = 10^{22}$ Pa s, shear stress is increased (Fig. 3e) and the thickness of layer S is also increased (Fig. 3f). This indicates that to produce dislocation creep in asthenosphere, the asthenospheric viscosity cannot be too small. For an asthenospheric viscosity significantly smaller than 10^{19} Pa s, stress will be reduced to the point that no dislocation creep channel will form. We will discuss this further in later sections. While dislocation creep produces LPO, diffusion creep can destroy existing LPO. In most cases with high viscosity, strain by diffusion creep deformation is limited at shallow depths and LPO is not destroyed by diffusion creep that takes place subsequent to dislocation creep deformation. However, for a small enough viscosity (e.g. $\eta_{ref} = 10^{20}$ Pa s), strain by diffusion creep at the shallow depths may be significant enough to destroy LPO. Although we do not know very well to what degree diffusion creep can destroy LPO, we attempt to illustrate the effect in the following way. Similar to calculating the thickness of layer S, we calculate diffusion creep strain by integrating strain rate at depths where diffusion creep occurs following dislocation creep. We assume that strain by diffusion creep greater than 0.5 will completely destroy any existing LPO. The thickness of the diffusion creep strain layer is subtracted from the thickness of S to obtain the thickness of the anisotropic layer remaining after diffusion creep has destroyed some of the existing LPO (thick dashed line in Fig. 3f). After ~ 50 Myr, strain by diffusion creep has accumulated sufficiently to begin to destroy LPO and the thickness of the anisotropic layer decreases with time.

We now explore the effects of varying τ_{Tref} (Figs 4(a), (b) and (c)). With $\tau_{Tref} = 40$ MPa, τ_T has a minimum value of ~ 1 MPa at a depth of ~ 100 km (Fig. 4b). The increased τ_T leads to a thinner channel of dislocation creep and larger viscosity in the asthenosphere compared with the reference case. The increased viscosity also results in increased shear stress (Fig. 4b). As expected, the thickness of layer S decreases with increasing τ_T (Fig. 4c). The viscosity is not depressed in the asthenosphere as much as in the reference case with a lower transition stress (Fig. 4a) because of the reduced dislocation creep deformation (i.e. non-Newtonian deformation).

In Figs 4(d), (e) and (f), the activation volume for dislocation creep, V_1 , is changed to 11 cm³ mol⁻¹. Since transition stress is fixed to τ_{Tref} at $z = z_0$, decreasing V_1 has the effect of raising transition stress in the asthenosphere (Fig. 4e). Decreasing V_1 results in an increase of the stress term of eq. (7), which increases viscosity in the dislocation creep channel (Fig. 4d). Consequently, shear stress is also increased (Fig. 4e). However, the net effect is that the thickness of layer S is decreased for decreased V_1 (Fig. 4f).

Although these calculations show that the strength of anisotropy is sensitive to τ_{Tref} , η_{ref} and V_1 , the controlling parameters seem to be τ_T and η in the asthenosphere. For a given U_p , a smaller asthenospheric viscosity results in a smaller stress, which hinders dislocation creep. On the other hand, a smaller transition stress in the asthenosphere favours dislocation creep. We explored the parameter space to identify trends in thickness of layer S (Fig. 5) as asthenospheric viscosity and transition stress were varied. The minimum (i.e. asthenospheric) values of viscosity and transition stress (η_{min} and τ_{Tmin}) have been used for the vertical and horizontal

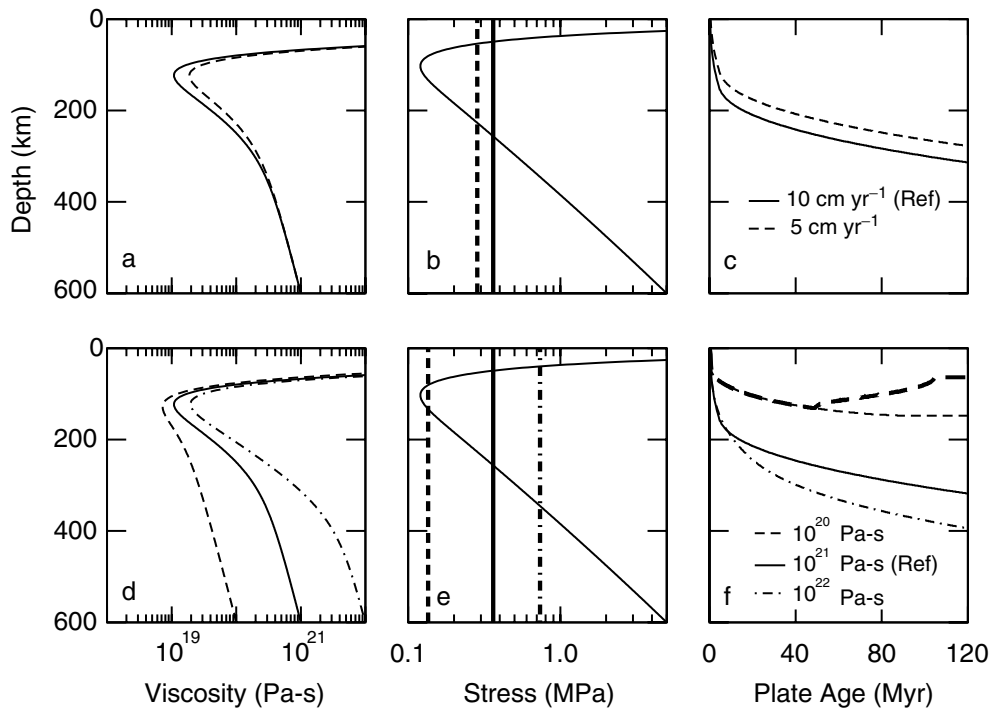


Figure 3. Results of model calculations varying U_p (a, b, c) and η_{ref} (d, e, f). Solid lines are the reference for lithospheric age of 40 Myr in all plots. Solid and dashed lines indicate results of varying U_p and η_{ref} . (c) and (f) are for layer S. See Fig. 2 for details.

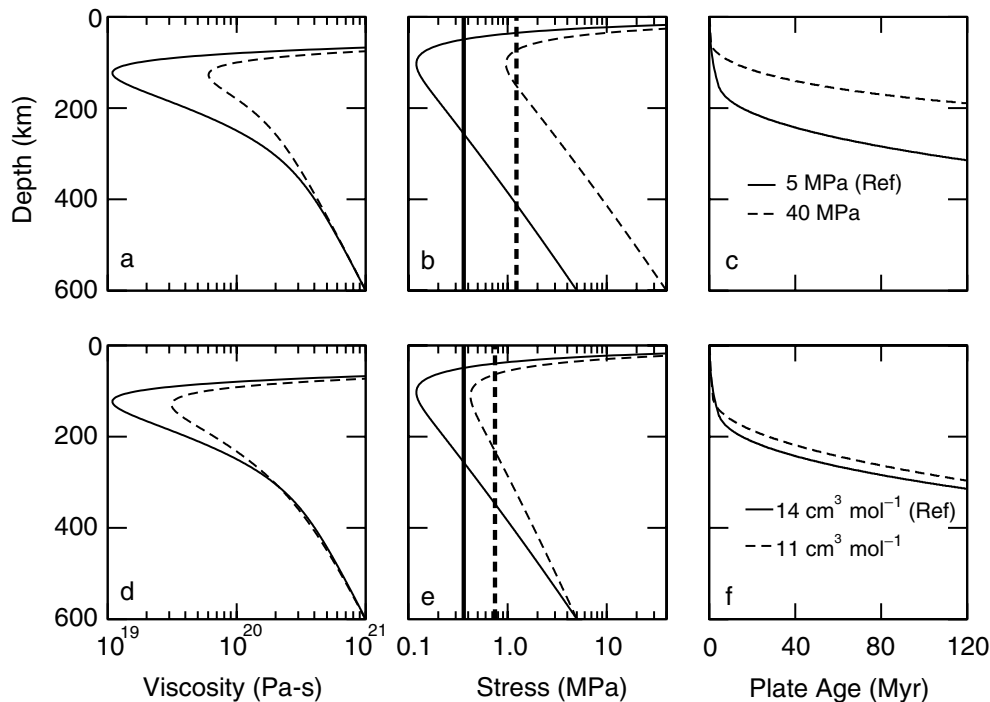


Figure 4. Results of model calculations varying τ_{Tref} (a, b, c) and V_1 (d, e, f). Solid lines are the reference for lithospheric age of 40 Myr in all plots. Solid and dashed lines indicate results of varying τ_{Tref} and V_1 . (c) and (f) are for layer S. See Fig. 2 for details.

axes respectively in Fig. 5. For a given pair of η_{min} and τ_{Tmin} , the thickness of S increases from 40 to 120 Myr (Figs 5a and b). Reducing V_1 increases the thickness of S (Fig. 5c), while reducing U_p reduces the thickness of S (Fig. 5d). We limited η_{ref} to a maximum of 10^{22} Pa s. Thus, for a given τ_{Tmin} , there is a maximum η_{min} . The

stippled region is beyond this maximum and is not considered in the current study. These results show that a channel of dislocation creep may never form for too small an asthenospheric viscosity or too large an asthenospheric transition stress (i.e. the white region to the lower right of all plots of Fig. 5). For $U_p = 10 \text{ cm yr}^{-1}$, our results

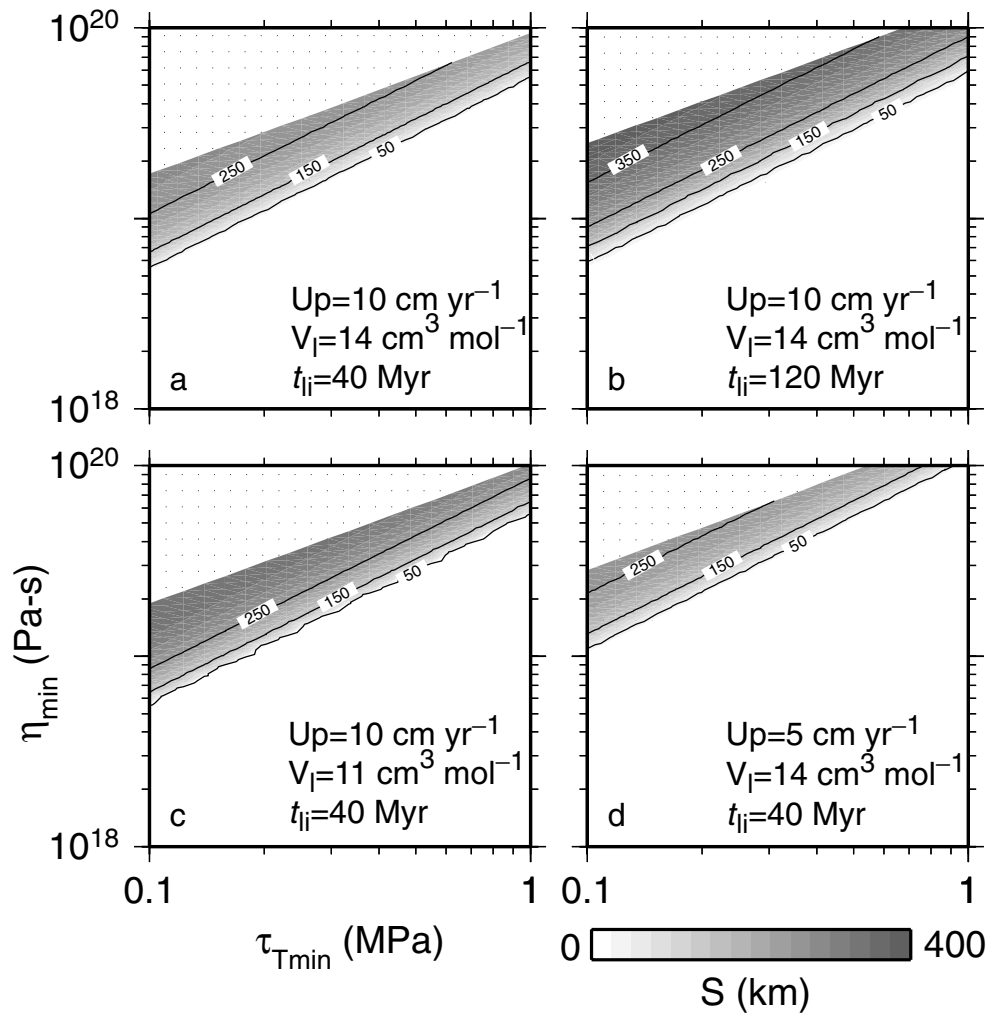


Figure 5. Parameter space maps of layer thickness for layer S. In the white lower region, no S layer is formed. The stippled region is beyond the maximum η_{\min} (no calculations done in this region). (a, b) Reference case for ages 40 Myr and 120 Myr. (c, d) Same as reference but with a lower V_l or smaller U_p .

for different parameters show that asthenospheric viscosity needs to be greater than 5×10^{18} Pa s to produce any significant dislocation deformation (Figs 5a–c), if the asthenospheric transition stress is greater than 0.1 MPa (Hirth & Kohlstedt 2003). This minimum asthenospheric viscosity needs to be larger for larger transition stress (e.g. Fig. 5a) or smaller plate motion (Fig. 5d).

3.3 Effects of a high-viscosity lid

Partial melting may lead to an increase in mantle viscosity due to the release of volatiles (Karato 1986). Hirth & Kohlstedt (1996) suggested that the increase in viscosity for the top 70 km of oceanic lithosphere may be as large as a factor of 500, as a result of melting and the formation of the oceanic crust at spreading centres. Here we explored the implications of a 70 km thick high-viscosity upper layer. In our calculations, all parameters are identical to the reference case, but the viscosity above 70 km was multiplied by a factor of 500 (Figs 6a and 2a). Consequently, transition stress remains the same as in the reference case (Figs 6b and 2b).

The effect of this high-viscosity layer is to inhibit deformation within the layer, thus reducing strain there (Figs 6d and e). The bottom of the strain curves for 40 and 120 Myr are nearly the same as the reference case without a dry layer (Figs 6e and 2e), with

strain increasing from 0 to 1.0 over 12 km for 40 Myr and over 5 km for 120 Myr. Unlike the reference case, the top of the strain curve is very flat, indicating a sharp transition into the anisotropic layer (Fig. 6e). Since deformation is limited to depths greater than 70 km, the thickness of layer S is reduced, compared with the reference case (Figs 6f and 2f).

Notice that because stress is constant, dislocation creep still dominates above 70 km for ages less than ~ 50 Myr (Fig. 6c). However, the high viscosity in the top 70 km makes it impossible to produce significant dislocation strain within the top layer. Layer D has roughly the same thickness as the reference case for lithosphere older than ~ 30 Myr, but for lithosphere younger than ~ 30 Myr, the thickness of layer D is increased compared with the reference case (Figs 6c and 2c). This is because for young lithosphere the increased viscosity in the top layer affects the overall mantle viscosity and increases shear stress, thus increasing the thickness of layer D. For old lithosphere, the dislocation creep channel exists entirely below 70 km and is unaffected by the high-viscosity upper layer (Fig. 6c).

4 DISCUSSIONS AND CONCLUSION

We have investigated the dependence of dislocation creep deformation in the oceanic upper mantle on mantle rheology with a

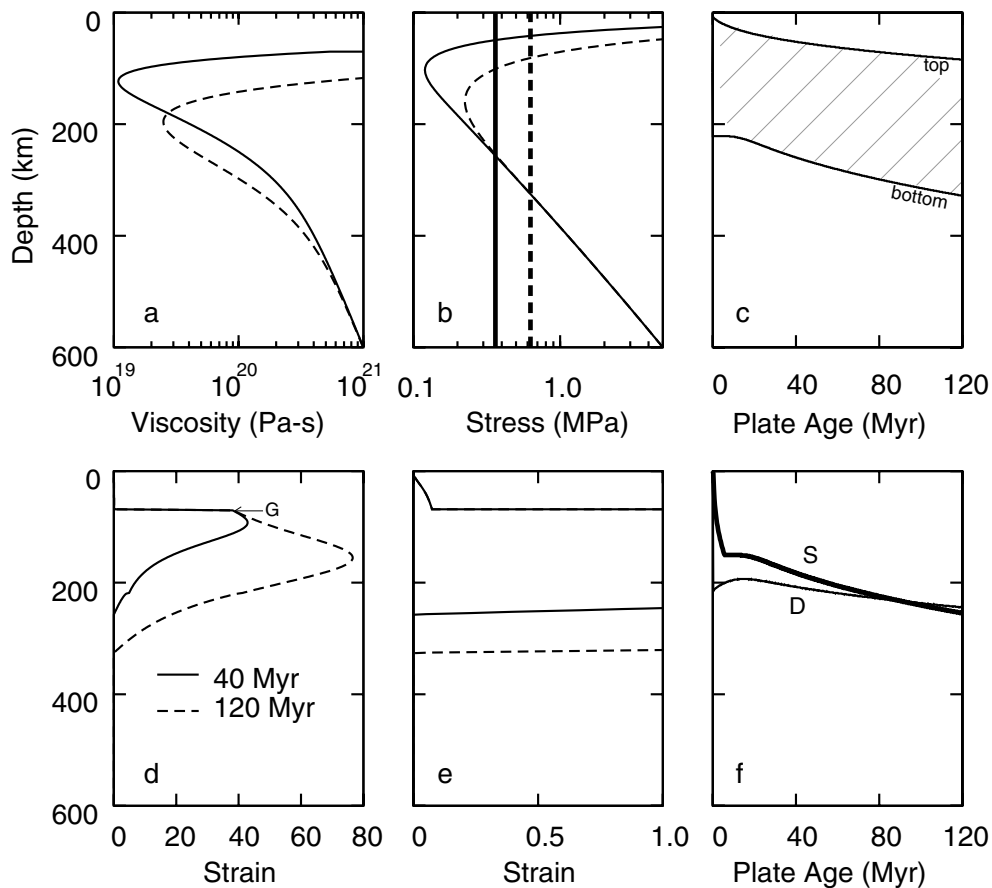


Figure 6. Results of including a 70 km thick high-viscosity lid but otherwise same as Fig. 2. See Fig. 2 for descriptions.

simple dynamic model that couples plate motion, mantle stress and a composite rheology (i.e. both Newtonian and non-Newtonian rheologies). The main findings can be summarized as follows.

(1) Using the experimentally determined rheological parameters, our models predict a ~ 200 km thick layer in the upper mantle with significant dislocation deformation for reasonable model parameters including plate motion of 10 cm yr^{-1} , asthenospheric viscosity of 10^{19} Pa s and asthenospheric transition stress of $\sim 0.1 \text{ MPa}$ (Figs 5a–c). The thickness of this dislocation deformation layer is broadly consistent with the thickness of anisotropic layer inferred from the seismic studies (e.g. Ekstrom & Dziewonski 1998).

(2) To produce any significant dislocation creep deformation, and hence anisotropy, in the upper mantle, asthenospheric viscosity needs to be greater than $5 \times 10^{18} \text{ Pa s}$ for plate motion of 10 cm yr^{-1} and asthenospheric transition stress of $\sim 0.1 \text{ MPa}$. For slower plate motion or larger transition stress, the asthenospheric viscosity needs to be larger (Fig. 5).

(3) Slower plate motion leads to a thinner layer of dislocation creep deformation (i.e. weaker seismic anisotropy) and higher viscosity in the upper mantle (Figs 3a–c). This is consistent with the observed asymmetry in seismic anisotropy across the EPR (Wolfe & Solomon 1998).

(4) Our plate shear models indicate that the strength of dislocation creep always increases with lithospheric age (Fig. 2f). If the reduced strength of seismic anisotropy below the relatively old Pacific Plate revealed in Montagner (2002) and Becker *et al.* (2003) is robust, this indicates that other processes including small-scale convection, plume-driven mantle flow (Becker *et al.* 2003; Gaboret

et al. 2003) or the presence of significant fossil anisotropy with a direction which is not parallel to the dynamic anisotropy may play a significant role in altering the deformation field imposed by plate motion.

(5) When a high-viscosity lid is present, deformation in the lid is inhibited and significant dislocation creep deformation induced by plate shear can only take place below the lid (Figs 6d–e). If the lid is created as a result of crust-forming processes in spreading centres, then any significant deformation and anisotropy at the shallow depths in the lid may be required to form in the spreading centres where the melting is active.

Our results have a number of important implications for the dynamics and structure of the oceanic upper mantle. Our study demonstrates that there is an important relation between the thickness of the anisotropic layer, asthenospheric viscosity and transition stress, all of which can be studied independently via field observations and laboratory studies. As our understanding of the transition stress and seismic anisotropy improves, they may be used to constrain the asthenospheric viscosity, a parameter that is important to many geodynamic problems.

Our results show that the strength of anisotropy depends on plate motion. Slower plate motion gives rise to weaker anisotropy. Its relative effects are much larger for young lithosphere than for old lithosphere (Fig. 3c). This suggests that at least part of the asymmetry in the seismic anisotropy across the EPR may be explained simply as the consequence of asymmetric spreading velocity on each side of the EPR, thus raising the question of to what extent the

asthenospheric return flow suggested by Wolfe & Solomon (1998) is needed.

Similar to the work of Karato & Wu (1993), our models also predict that dislocation creep only operates at certain depths in a layer that is always below the surface layer in which the deformation is dominated by diffusion creep (Fig. 2c). This shallow layer with diffusion creep is consistent with the lack of correlation between the observed elastic thickness at seamounts and seamount heights (Watts & Zhong 2000). Elastic thickness appears to be dependent only on lithospheric age (i.e. thermal structure) at the time of loading (Watts *et al.* 1980). The physics of stress relaxation suggests that elastic thickness is ultimately controlled by the viscosity structure of the lithosphere. This is because the viscosity determines how stress relaxes in the lithosphere and how the seamounts are supported (e.g. Watts & Zhong 2000). If the deformation of oceanic lithosphere at the depths that define the elastic thickness is controlled by dislocation creep, we would expect that for seamounts loading on lithosphere with the same age, the elastic thickness correlates with seamount height, because a higher seamount would lead to larger lithospheric stress that with stress-dependent dislocation creep deformation would result in a weaker lithosphere or a thinner elastic plate. However, the observed elastic thicknesses at seamounts and oceanic islands with vastly different heights do not show any correlation with seamount heights. Diffusion creep, on the other hand, explains this observation well, because it does not depend on stress.

Our results with a high-viscosity lid simulating the effects of dehydration on mantle viscosity (Karato 1986; Hirth & Kohlstedt 1996) may have implications for the nature of the Gutenberg discontinuity that is often observed in the oceanic upper mantle (e.g. Revenaugh & Jordan 1991). Karato (1995) showed that water content has important effects on seismic velocities. Gaherty *et al.* (1998) built on this idea, suggesting that the Gutenberg discontinuity may be related to the formation of the high-viscosity lid as a result of melting and crust-forming processes at the spreading centres. Gung *et al.* (2003) proposed that the Gutenberg discontinuity may mark the boundary for seismic anisotropy. Our results show that dislocation creep deformation increases sharply at the base of the high-viscosity lid (Figs 6d–e), which is consistent with the proposals of Gaherty *et al.* (1998) and Gung *et al.* (2003).

Despite the important implications of our simple models for the dynamics and structure of the oceanic upper mantle, we wish to point out potential caveats of our approach that should be improved in future studies with fully numerical modelling. First, our model with only plate shear may not be suited for young lithosphere where vertical flow is equally important. This is particularly relevant to studying mantle anisotropy below young lithosphere (e.g. Wolfe & Solomon 1998) and at very shallow depths which may be mainly caused by crust-forming processes. Secondly, 2-D and 3-D effects may also play certain roles in producing vertical variations in stress, especially when other processes including plume-driven flow and sublithospheric small-scale convection are important, which will also complicate the strain evolution. Third, we did not consider other potentially relevant deformation processes including dynamic recrystallization (Kaminski & Ribe 2001; Zhang & Karato 1995; Montesi & Hirth 2003) which should be considered in future studies when the physics of these processes is better understood.

ACKNOWLEDGMENTS

We thank S. Karato and N. Ribe for constructive reviews. This research is supported by David and Lucile Packard Foundation and NSF under grant number EAR-0134939.

REFERENCES

- Becker, T.W., Kellogg, J.B., Ekstrom, G. & O'Connell, R.J., 2003. Comparison of azimuthal seismic anisotropy from surface waves and finite-strain from global mantle-circulation models, *Geophys. J. Int.*, **155**, 696–714.
- Bjarnason, I.T., Silver, P.G., Rumpker, G. & Solomon, S.C., 2002. Shear wave splitting across the Iceland hot spot: results from the ICEMELT experiment, *J. geophys. Res. Solid Earth*, **107**, (B12), art. No. 2382
- Blackman, D.K., Wenk, H.R. & Kendall, J.M., 2002. Seismic anisotropy of the upper mantle 1. Factors that affect mineral texture and effective elastic properties, *Geochem. Geophys. Geosyst.*, **3**, (9), 8601
- Davaille, A. & Jaupart, C., 1994. Onset of thermal convection in fluids with temperature dependent viscosity—application to the oceanic mantle, *J. geophys. Res. Solid Earth*, **99** (B10), 19 853–19 866.
- Dziewonski, A.M. & Anderson, D.L., 1981. Preliminary reference earth model, *Phys. Earth planet. Inter.*, **25**, (4), 297–356.
- Ekstrom, G. & Dziewonski, A.M., 1998. The unique anisotropy of the Pacific upper mantle, *Nature*, **394**, 168–172.
- Forte, A.M. & Mitrovica, J.X., 1997. A resonance in the Earth's obliquity and precession over the past 20 Myr driven by mantle convection, *Nature*, **390**, (6661), 676–680.
- Gaboret, C., Forte, A.M. & Montagner, J.P., 2003. The unique dynamics of the Pacific Hemisphere mantle and its signature on seismic anisotropy, *Earth planet. Sci. Lett.*, **208**, (3–4), 219–233.
- Gaherty, J.B., Kato, M. & Jordan, T.H., 1998. Seismological structure of the upper mantle: a regional comparison of seismic layering, *Phys. Earth planet. Int.*, **110**, 21–41.
- Gung, Y.C., Panning, M. & Romanowicz, B., 2003. Global anisotropy and the thickness of continents, *Nature*, **422**, (6933), 707–711.
- Hager, B.H., 1991. Mantle viscosity: a comparison of models from post-glacial rebound and from the geoid, plate driving forces, and advected heat flux, in *Glacial Isostasy, Sea level and Mantle Rheology*, pp. 493–513. eds Sabadini, R., Lambeck, K. & Boschi, E., Kluwer Academic Publishers, Dordrecht.
- Hager, B.H. & Richards, M.A., 1989. Long-wavelength variations in Earth's geoid—physical models and dynamical implications, *Phil. Trans. R. Soc. Lond. A*, **328**, (1599), 309–327.
- Hall, C.E. & Parmentier, E.M., 2003. Influence of grain size evolution on convective instability, *Geochem. Geophys. Geosyst.*, **4**, doi:10.1029/2002GC000308.
- Hirth, G., 2002. Laboratory constraints on the rheology of the upper mantle, *Rev. Mineral. Geochem.*, **51**, 97–120.
- Hirth, G. & Kohlstedt, D.L., 1996. Water in the oceanic upper mantle: Implications for rheology, melt extraction and the evolution of the lithosphere, *Earth planet. Sci. Lett.*, **144**, (1–2), 93–108.
- Hirth, G. & Kohlstedt, D.L., 2003. The rheology of the upper mantle and the mantle wedge: a view from the experimentalists, Inside the Subduction Factory, AGU Geophysical Monograph Series, ed. Eiler, J., American Geophysical Union, Washington, DC (in press)
- Kaminski, E., & Ribe, N.M., 2001. A kinematic model for recrystallization and texture development in olivine polycrystals, *Earth planet. Sci. Lett.*, **189**, (3–4), 253–267.
- Karato, S., 1986. Does partial melting reduce the creep strength of the upper mantle, *Nature*, **319**, (6051), 309–310.
- Karato, S., 1995. Effects of water on seismic wave velocities in the upper mantle, *Proc. Japan. Acad. Ser. B*, **71**, 61–66.
- Karato, S. & Jung, H., 2003. Effects of pressure on high-temperature dislocation creep in olivine, *Phil. Mag.*, **83**, (3), 401–414.
- Karato, S. & Wu, P., 1993. Rheology of the upper mantle: a synthesis, *Science*, **260**, 771–778.
- Korenaga, J. & Jordan, T. H., 2002. On 'steady-state' heat flow and the rheology of oceanic mantle, *Geophys. Res. Lett.*, **29**, (22), art. no. 2056
- Kubo, A. & Hiramatsu, Y., 1998. On the presence of seismic anisotropy in the asthenosphere beneath continents and its dependence on plate velocity: significance of reference frame selection, *Pure appl. Geophys.*, **151**, 281–303.

- McKenzie, D., 1979. Finite deformation during fluid-flow, *Geophys. J. R. astr. Soc.*, **58**, (3), 689–715.
- McNamara, A.K., van Keken, P.E. & Karato, S., 2002. Development of anisotropic structure in the Earth's lower mantle by solid-state convection, *Nature*, **416**, 310–314.
- McNamara, A.K., van Keken, P.E. & Karato, S., 2003. Development of finite strain in the convecting lower mantle and its implications for seismic anisotropy, *J. geophys. Res.*, **108**, (B5), 2230, doi:10.1029.2002JB001970.
- Montagner, J.P., 2002. Upper mantle low anisotropy channels below the Pacific Plate, *Earth planet. Sci. Lett.*, **202**, 263–274.
- Montagner, J.P. & Tanimoto, T., 1991. Global upper mantle tomography of seismic velocities and anisotropies, *J. geophys. Res. Solid Earth*, **96**, (B12), 20 337–20 351.
- Montesi, L.G.J. & Hirth, G., 2003. Grain size evolution and the rheology of ductile shear zones: from laboratory experiments to postseismic creep, *Earth planet. Sci. Lett.*, **211**, 97–110.
- Nicolas, A. & Christensen, N.I., 1987. Formation of anisotropy in upper mantle peridotites—a review, in *Composition, Structure, and Dynamics of the Lithosphere–Asthenosphere System*, AGU Geodynamics Series 16, pp. 111–123, eds Fuchs, K. & Froidevaux, C., American Geophysical Union, Washington, DC.
- Parmentier, E.M., Turcotte, D.L. & Torrance, K.E., 1976. Studies of finite amplitude non-newtonian thermal convection with application to convection in the earth's mantle, *J. geophys. Res.*, **81**, 1839–1846.
- Pollitz, F.F., Burgmann, R. & Romanowicz, B., 1998. Viscosity of oceanic asthenosphere inferred from remote triggering of earthquakes, *Science*, **280**, (5367), 1245–1249.
- Revenaugh, J., & Jordan, T.H., 1991. Mantle layering from SCS reverberations.3. The upper mantle, *J. geophys. Res. Solid Earth*, **96**, (B12), 19 781–19 810.
- Ribe, N.M., 1992. On the relation between seismic anisotropy and finite strain, *J. geophys. Res. Solid Earth*, **97**, (B6), 8737–8747.
- Silver, P.G. & Holt, W.E., 2002. The mantle flow field beneath western North America, *Science*, **295**, (5557), 1054–1057.
- Simons, M. & Hager, B., 1997. Localization of the gravity field and the signature of glacial rebound, *Nature*, **390**, (6659), 500–504.
- Turcotte, D. & Schubert, G., 2002. *Geodynamics*, Cambridge University Press, Cambridge.
- Van den Berg, A.P., van Keken, P.E. & Yuen, D.A., 1993. The effects of a composite non-Newtonian and Newtonian rheology on mantle convection, *Geophys. J. Int.*, **115**, 62–78.
- Watts, A.B. & Zhong, S., 2000. Observations of flexure and the rheology of oceanic lithosphere, *Geophys. J. Int.*, **142**, (3), 855–875.
- Watts, A.B., Bodine, J.H. & Steckler, M.S., 1980. Observations of flexure and the state of stress in the oceanic lithosphere, *J. geophys. Res.*, **85**, 6369–6376.
- Wenk, H.R. & Christie, J.M., 1991. Comments on the interpretation of deformation textures in rocks, *J. struct. Geol.*, **13**, 1091–1110.
- Wolfe, C.J. & Solomon, S.C., 1998. Shear-wave splitting and implications for mantle flow beneath the MELT region of the East Pacific Rise, *Science*, **280**, 1230–1232.
- Zhang, S.Q. & Karato, S., 1995. Lattice preferred orientation of olivine aggregates deformed in simple shear, *Nature*, **375**, (6524), 774–777.
- Zhong, S. & Watts, A.B., 2002. constraints on the dynamics of mantle plumes from uplift of the Hawaiian Islands, *Earth. planet. Sci. Lett.*, **203**, (91), 105–116.